IOPscience iopscience.iop.org

Home Search Collections Journals About Contact us My IOPscience

Dynamic analysis of globular metal transfer in gas metal arc welding - a comparison of numerical and experimental results

This article has been downloaded from IOPscience. Please scroll down to see the full text article.

1998 J. Phys. D: Appl. Phys. 31 2929

(http://iopscience.iop.org/0022-3727/31/20/029)

View the table of contents for this issue, or go to the journal homepage for more

Download details:
IP Address: 129.119.132.10
The article was downloaded on 27/06/2012 at 22:48

Please note that terms and conditions apply.

J. Phys. D: Appl. Phys. **31** (1998) 2929–2941. Printed in the UK PII: S0022-3727(98)95240-8

Dynamic analysis of globular metal transfer in gas metal arc welding—a comparison of numerical and experimental results

H G Fan and R Kovacevic

Department of Mechanical Engineering, Southern Methodist University, 3160 SMU Boulevard, Dallas, TX 75205, USA

Received 19 June 1998

Abstract. A mathematical model to describe the globular transfer in gas metal arc welding is developed. This work is both theoretical and experimental. Using the volume-of-fluid (VOF) method, the fluid-flow and heat-transfer phenomena during the impingement of a droplet on a solid substrate, arc striking, the impingement of multiple droplets on the molten pool and finally the solidification after the arc extinguishes are dynamically studied. A He–Ne laser in conjunction with the shadow-graphing technique is used to observe the metal-transfer processes. Theoretical predictions and experimental results are shown to be in good agreement, suggesting that the theoretical treatment of the model is sound.

Nomenclature

a_d	droplet's acceleration in arc plasma
B_θ	azimuthal magnetic field
C_p	heat capacity
D_d	droplet's diameter
f	droplet-transfer frequency
f_L	liquid fraction
F	volume of fluid
g	gravitational acceleration
h	specific enthalpy
h_c	combined heat-transfer coefficient at the surface
I	arc current
j_r, j_z	radial, axial current density
k	thermal conductivity
K	drag index in source term
K_{max}	maximum drag index
n	normal direction to surface
P	pressure
r_q, r_c	heat-, current-flux-distribution radius
r, z	radial, axial coordinate
s	tangential direction along the surface
S	source term
t	time
T	temperature
T_r	reference temperature
T_∞	surrounding temperature
T_l	liquidus temperature
T_m	melting temperature
T_s	solidus temperature
u, w	radial, axial velocity
U	arc voltage
V_i	initial velocity of droplet
V_n	normal velocity component at molten pool's surface
V_s	tangential velocity component at molten pool's surface
V_w	wire-feeding speed
ΔH	latent heat of fusion

Greek symbols

β	coefficient of thermal expansion
η	arc's efficiency
μ	viscosity
μ_0	permittivity of free space
ρ	density
σ	electrical conductivity
ϕ	potential
γ	surface tension
$\mathrm{d}\gamma/\mathrm{d}T$	temperature gradient of surface tension
ε	emissivity of body's surface

1. Introduction

In view of the significant effects of weld-pool convection on the microstructure and properties of the resultant weld, numerous investigators have attempted to calculate heat transfer and fluid flow in the weld pool, especially in gas tungsten arc welding (GTAW) [1–6]. For GTAW, convection in the weld pool is driven by a combination of

 © 1998 IOP Publishing Ltd

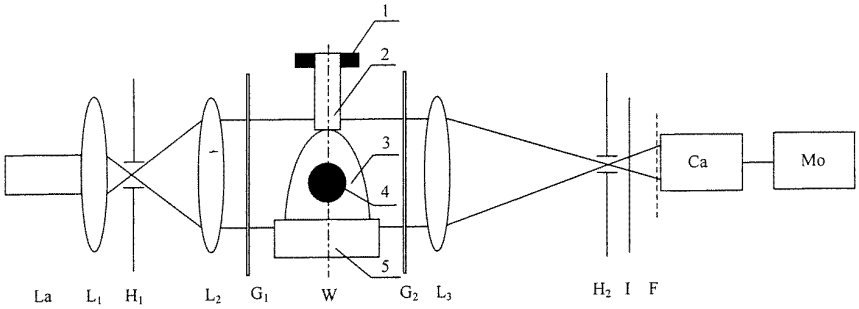

Figure 1. A schematic diagram of the photographic arrangement: La, laser; L_1, L_2 and L_3, lenses; H_1 and H_2, pin holes; G_1 and G_2, protective transparent screen glasses; I, image screen; F, filter; Ca, camera; Mo, monitor; and W, welding system (1, contact tube; 2, consumable electrode; 3, arc column; 4, droplet; and 5, workpiece).

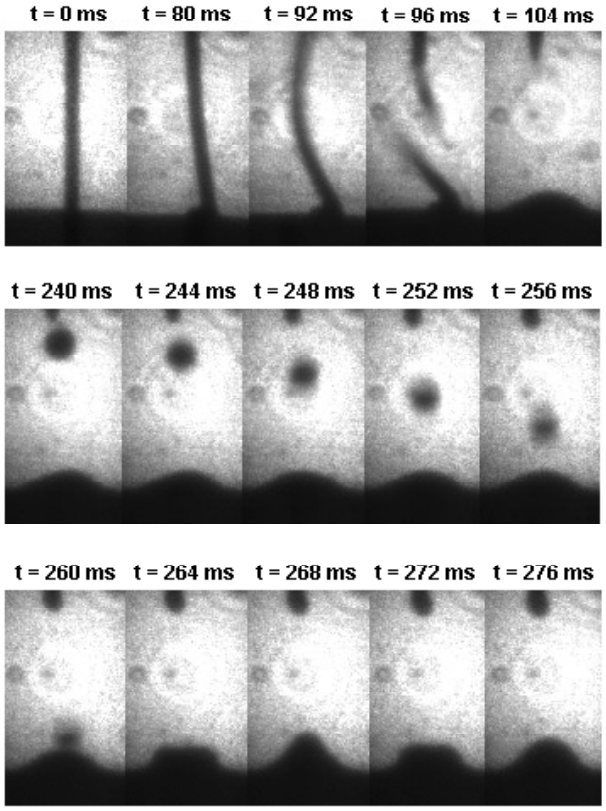

Figure 2. Successive images of arc striking and the impingement of the first droplet.

forces, which include the surface tension force, buoyancy force, electromagnetic force and arc drag force. In most cases, the fluid flow and heat transfer in the weld pool are controlled by the surface-tension force [7].

Gas metal arc welding (GMAW) is an arc welding process that uses an arc between a continuous, consumable filler metal electrode and the weld pool (figure 1). GMAW, due to its high productivity, has been the predominant welding process. Studying the transport phenomena in stationary GMAW could provide insight into what would happen in the molten pool with the impingement of multiple droplets. Compared with the GTA welding pool, however, the GMAW molten pool is less studied both in experimental and in theoretical aspects due to the interaction between the droplet and the base metal. The impingement of molten metal droplets into the weld pool in GMAW will affect the shape of the free surface and the convective heat transfer in the weld pool. Tsao and Wu [8] presented a two-dimensional stationary weld-pool-convection model for GMAW which assumed the weld pool's surface to be flat and took into account the exchange of thermal energy between metal droplets and the weld pool. Using boundary-fitted coordinates, Kim and Na [9] presented a three-dimensional quasi-steady model for the moving-bead-on-plate GMAW process. The size and profile of the weld pool were predicted, but the dynamic interaction between the droplet and the weld pool's free surface was not considered. Ushio and Wu [10] approximated the effect of the droplets on the weld pool as a constant force acting on the weld pool's free surface, although the impingement is not a continuous process. That is, the transient influence of successive impinging droplets on fluid flow in the weld pool was not considered. Choi *et al* [11] recently used the volume-of-fluid (VOF) method to simulate the short-circuit-mode metal transfer in stationary GMAW welding. However, the work did not include a description of thermal phenomena, rather it assumed that the droplets and molten pool were isothermal. Adopting the VOF method, Trapaga *et al* [12] simulated fluid flow, heat transfer and solidification of a single molten droplet impinging on a substrate in plasma spraying. However, the multiple droplets in GMAW produce much more complex phenomena which even involve electromagnetic forces and Marangoni flow.

To summarize, because of the complexity in accounting for the impingement of molten metal droplets on the surface of the weld pool, the existing models take a limited approach in dealing with the impingement of metal droplets by (i) accounting for an exchange of energy between the weld pool and the molten droplet, (ii) specifying a rate of addition of metal droplets, (iii) considering the dynamic interaction between the metal droplets and the free surface of the weld pool and (iv) considering the increase in volume of the weld pool due to the addition of molten metal droplets.

It is clear that the filler droplets have an important influence on the weld pool, since the droplets bring not only the impinging momentum but also a significant amount of thermal energy to the weld pool. Thus, one of the biggest challenges is the development of a realistic treatment of the impingement of the filler droplets into the weld pool,

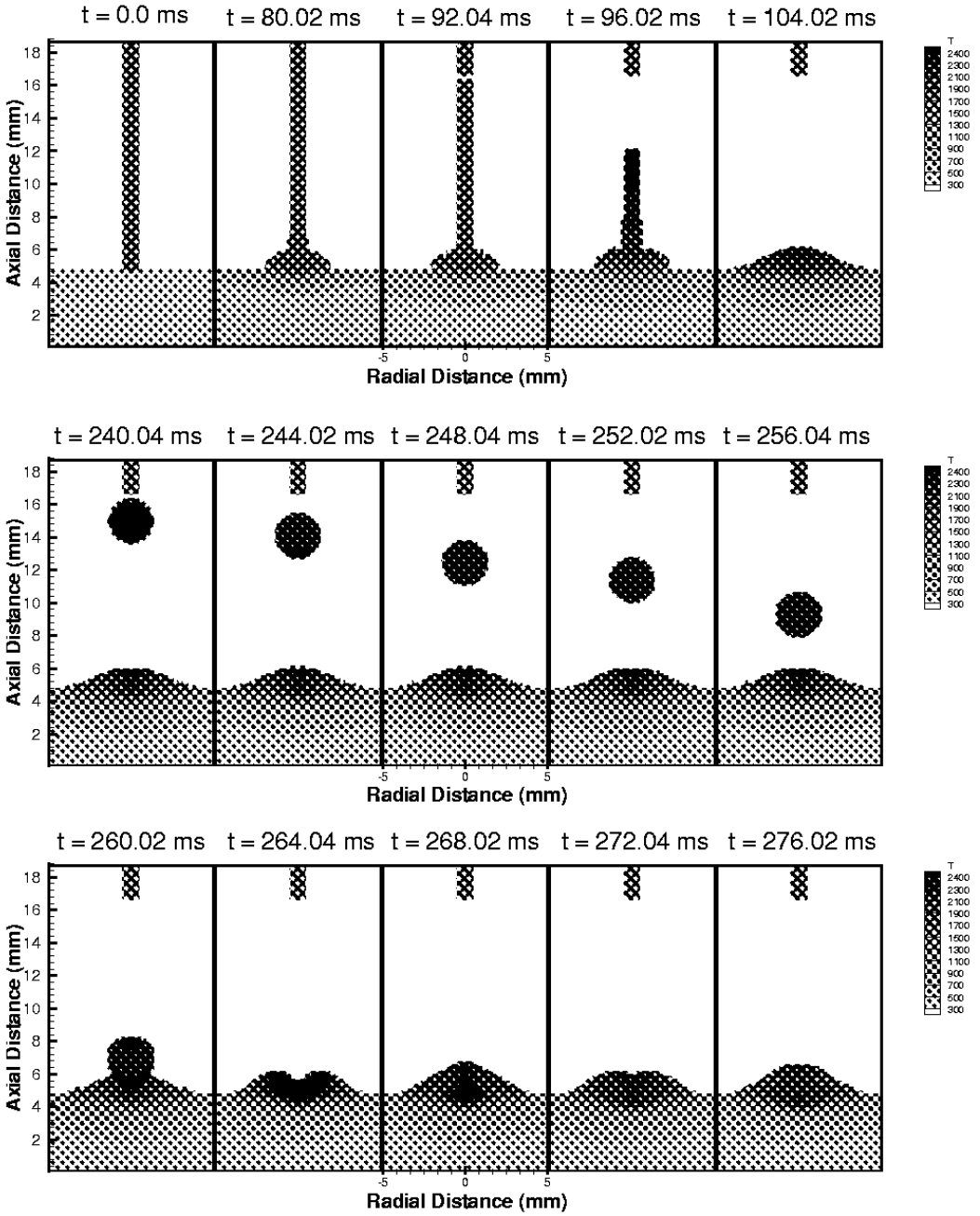

(a)

Figure 3. (a) The temperature distribution during the process of arc striking and the impingement of the first droplet on the molten pool. (b) The velocity distribution during the process of arc striking and the impingement of the first droplet on the molten pool.

Table 1. Welding parameters, some determined by measurements on high-speed films.

Case	I (A)	U (V)	V_w (m min^{-1})	D_d (mm)	V_i (m s^{-1})	a_d (m s^{-2})	f (drops s^{-1})
A	200	31	5.2	2.5	0.3	51	13
B	160	29	3.6	3.1	0.1	22	5

including the free surface's deformation. So far, no public literature has been published for GMAW considering the dynamic interaction between droplets and the molten pool. In this paper, a new transient two-dimensional model was developed to simulate the heat transfer and fluid flow associated with a weld pool into which molten droplets

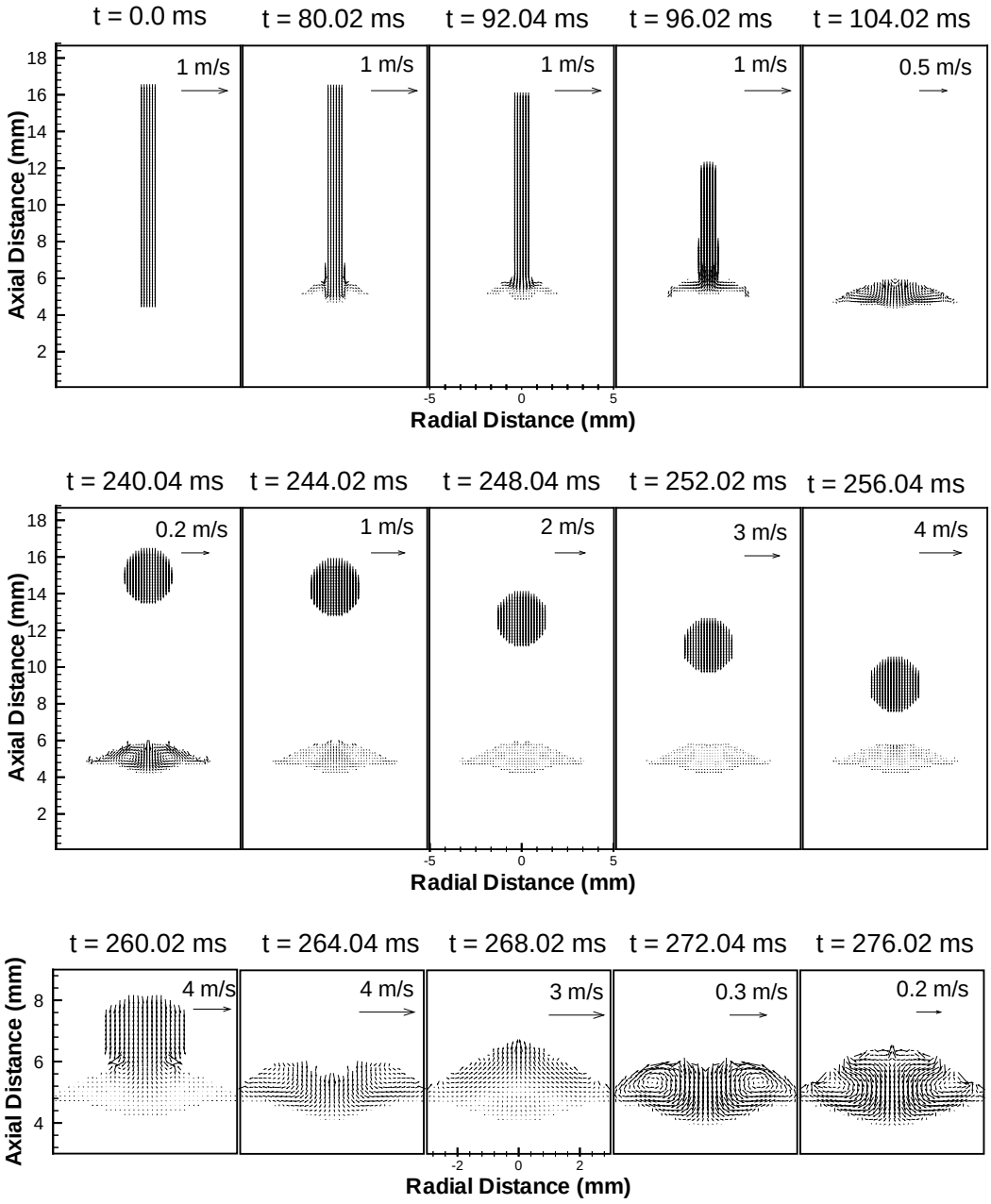

(b)

Figure 3. (Continued)

periodically are injected. The solution algorithm–volume of fluid (SOLA–VOF) [13], modified to include heat transfer and the electromagnetic force, was used to track the transiently deformed shape of the weld pool's surface. In addition, high-speed videography was used to record the welding process. The theoretical and experimental results were found to be in good agreement. A future model for GMAW should combine the electrode, arc plasma and molten pool, describing the growth and detachment of molten droplets [14], the transport and interaction of the molten droplets in the arc plasma and the interaction between the droplets and the weld pool.

2. Experimental procedures

In GMAW, there are various modes of metal transfer, classified into three main groups: free-flight transfer, bridging transfer and slag-protected transfer. In free-flight transfer, including globular, spray and explosive modes of transfer, the electrode does not come into contact with the molten pool. Lesnewich [15] showed that the mode of metal transfer depends on many operational variables such as the welding current, electrode's extension, electrode's diameter and polarity. Among these variables, the welding current is the most common variable that is adjusted to obtain the desired metal-transfer mode. At low welding

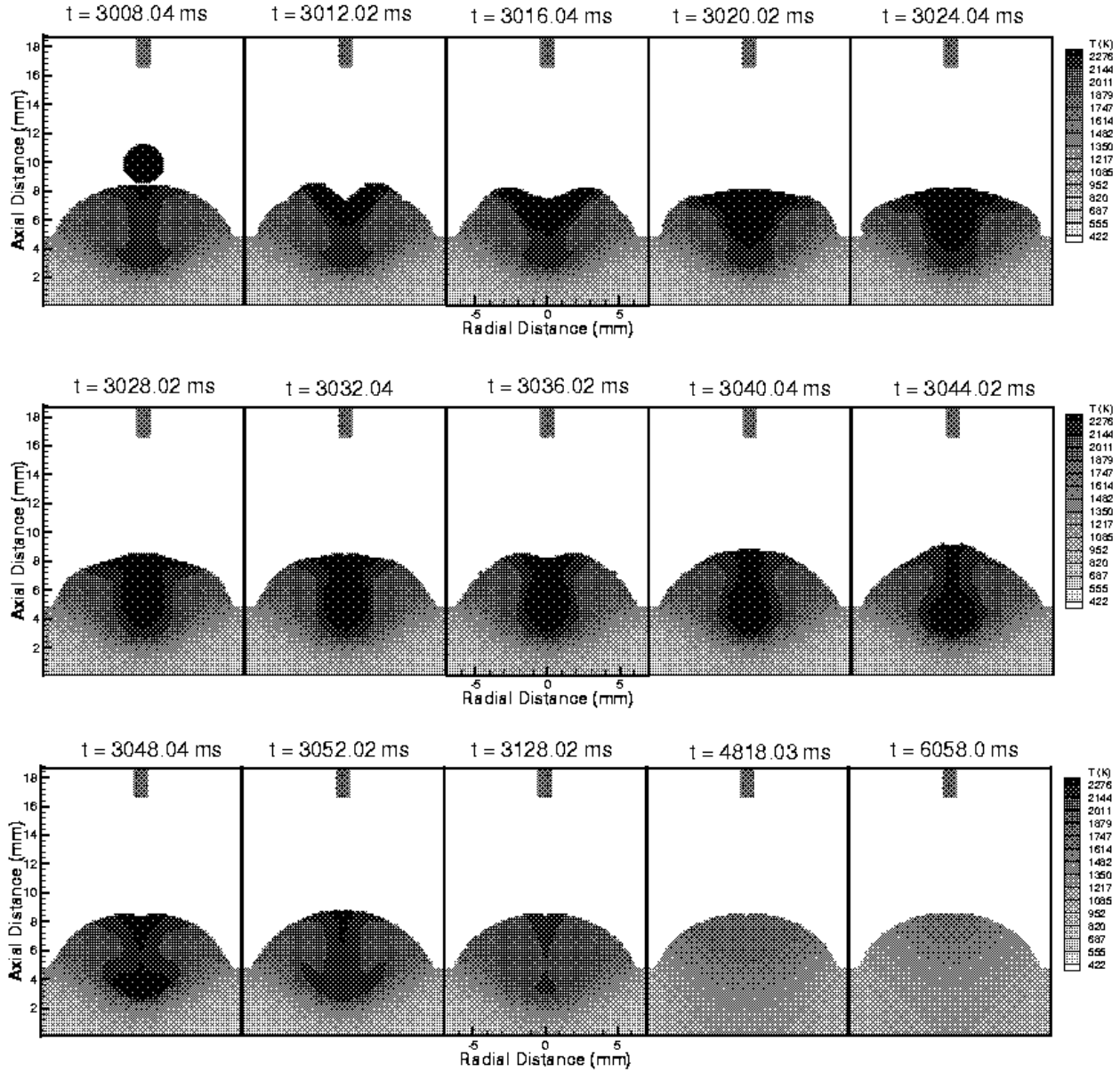

(a)

Figure 4. (a) The temperature distribution during the process of the impingement of the last droplet and subsequent solidification (case A). (b) The velocity distribution during the process of the impingement of the last droplet and subsequent solidification (case A).

currents, the globular transfer mode occurs, whereas the spray transfer mode occurs at relatively higher welding currents. There is a sudden change in rate of formation of droplets over a narrow current range, which is called the transition. According to Lesnewich's work, in carbon steel welding with 1.2 mm diameter electrodes, a transition in metal transfer occurred at approximately 250 A.

In the experiment, analysis of metal transfer was performed using high-speed videography with a laser-backlighted shadow-graphic method [16]. The set-up of the laser optics and the high-speed camera systems is shown in figure 1. A He–Ne laser was used as a background light source to exclude the high-intensity arc light. With the collimated light directed at the arc, a shadow graph of the droplet and molten pool was obtained. The high-speed video camera is capable of grabbing images at a maximum speed of 1000 full-frame pictures per second.

A power supply (Miller Phoenix^{TM} 456) set in the constant-current mode was used to make stationary spot welds on a 4.8 mm thick mild steel plate. The welding was performed under direct current, electrode negative conditions. The electrode used in this experiment was a mild steel welding wire with a diameter of 1.2 mm. The shielding gas used was pure argon. The length of the electrode's extension between the contact tube and the tip of the electrode was 16 mm. Other experimental conditions are given in table 1. The droplet's size (D_d) was measured from the still image on the screen and averaged. A number

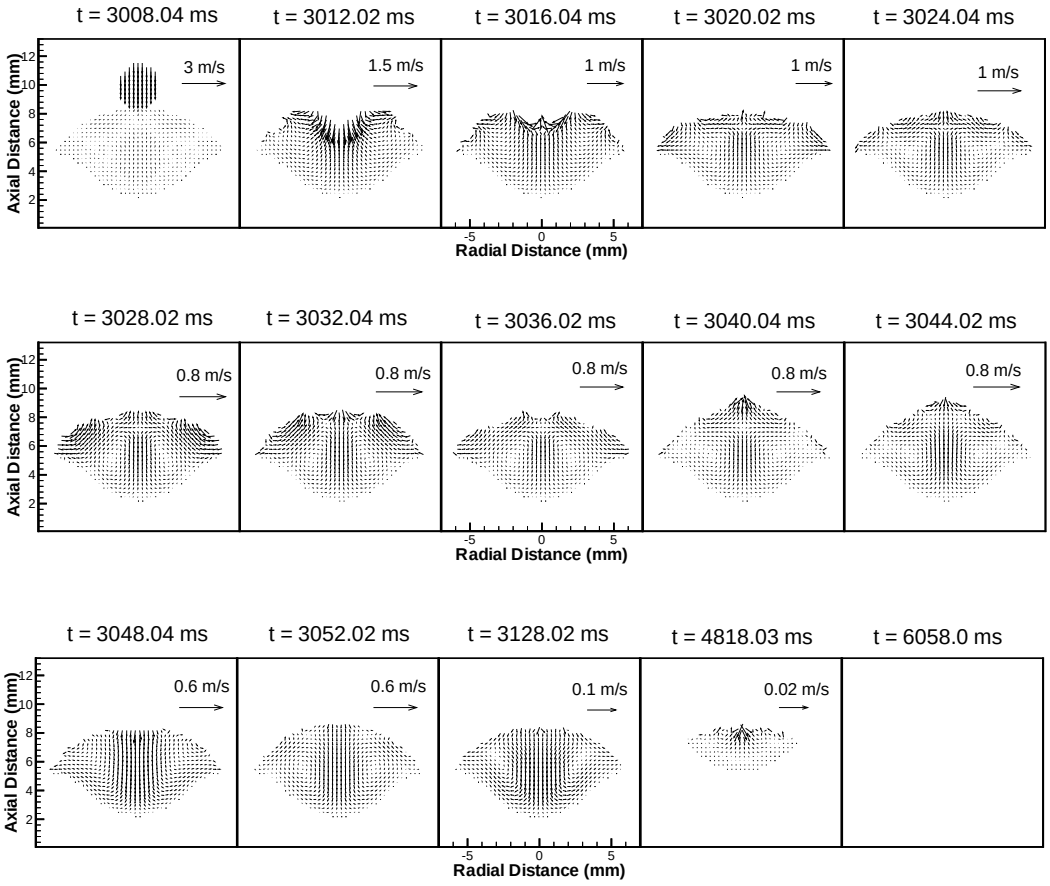

(b)

Figure 4. (Continued)

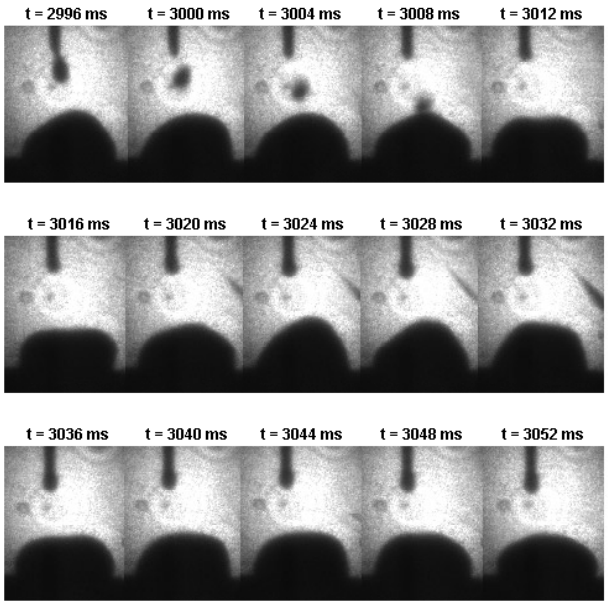

Figure 5. The images for the impingement of the last droplet on the molten pool (case A).

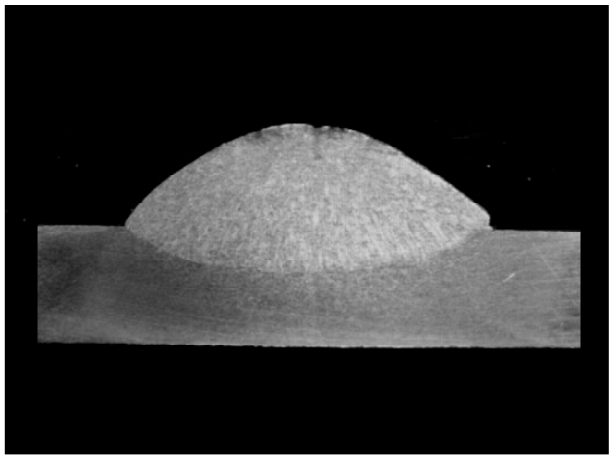

Figure 6. The resultant weld bead (case A).

of works [17] have shown that, in GMA welding, the drops detach from the electrode with an appreciable velocity and are further accelerated as they pass across the arc. Thus, the axial position, z, was measured on the images. The drop's velocity at detachment (V_i) and acceleration (a_d) were determined graphically from the axial position (z) versus time (t).

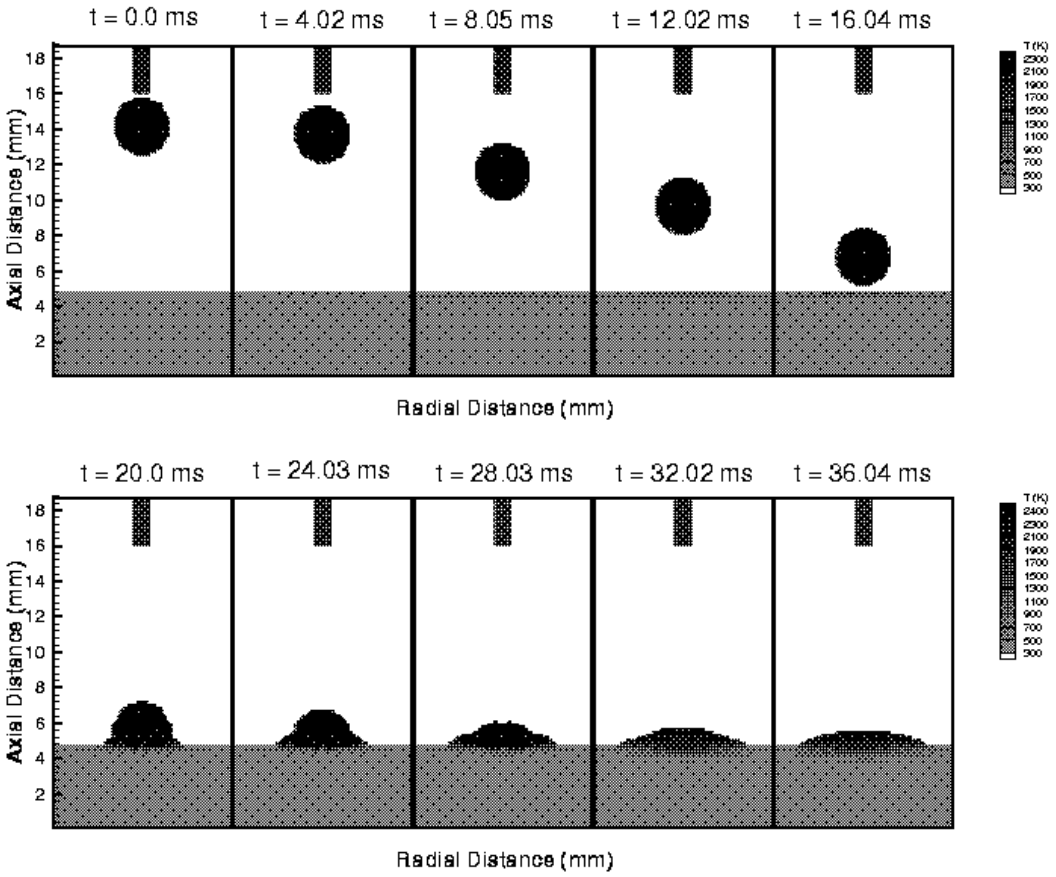

(a)

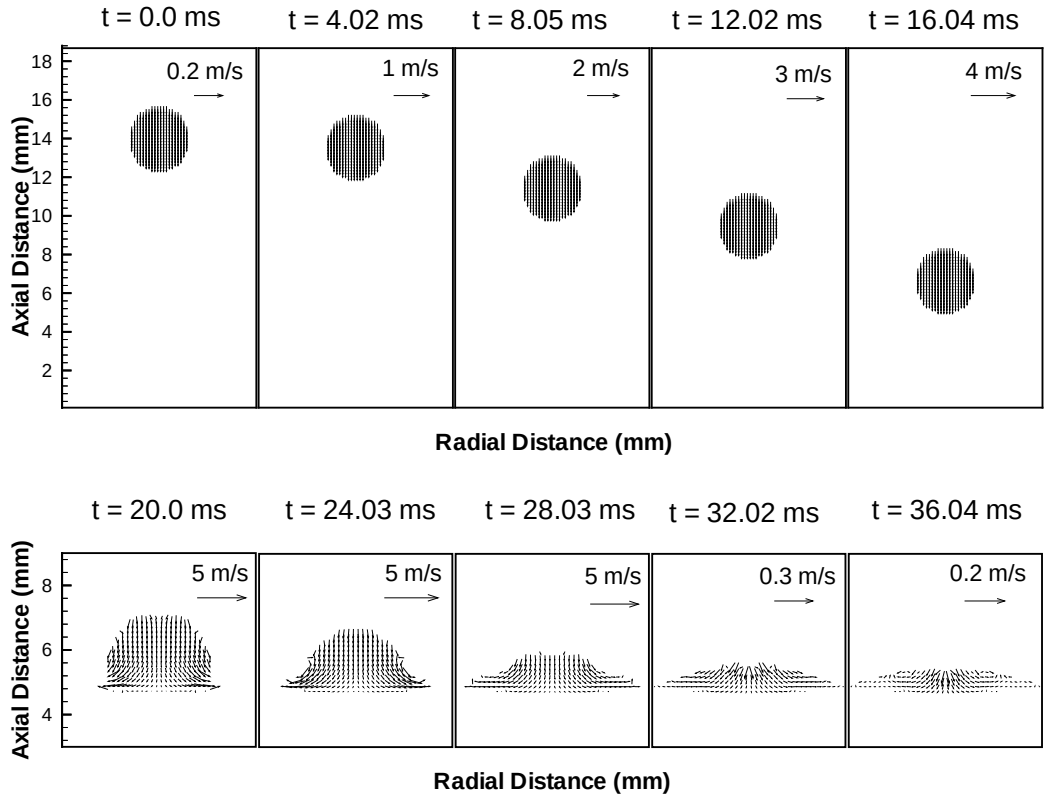

(b)

Figure 7. (a) The temperature distribution for the impingement of the droplet on the substrate. (b) The velocity distribution for the impingement of the droplet on the substrate.

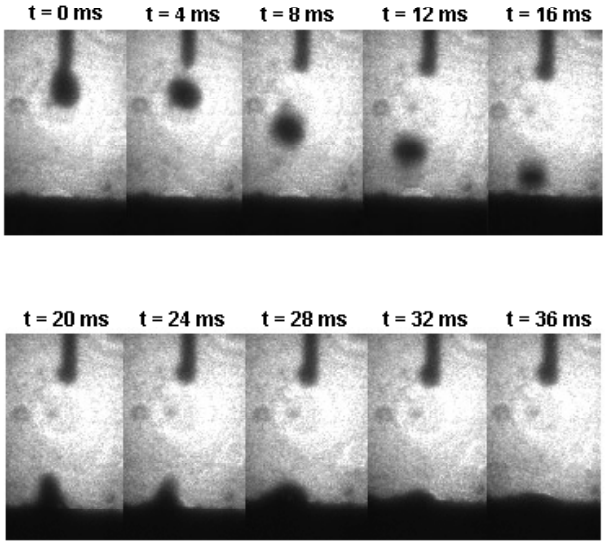

Figure 8. The images for the impingement of the droplet onto the substrate.

3. The mathematical formulation

3.1. Governing equations

In order to simplify the mathematical model, the following assumptions have been made.

(i) The droplet's impingement process is assumed to be axisymmetrical.

(ii) Laminar flow is assumed since the size of the pool is small.

(iii) The thermophysical properties which are listed in table 2 are assumed constant.

(iv) The fluid in the pool is driven by a combination of buoyancy, electromagnetic and surface tension forces.

(v) The droplet's diameter, initial velocity and acceleration are set according to the experimental results (table 1). The temperature of the droplet is assumed to be 2400 K [17, 20].

On the basis of the above assumptions, the governing differential equations used to describe heat and fluid flow in the weld pool can be expressed as follows.

The equation of mass continuity is

$$\frac{1}{r}\frac{\partial(ru)}{\partial r}+\frac{\partial w}{\partial z}=0. \tag{1}$$

Table 2. Physical properties of the workpiece.

Property	Value	Property	Value
β	$10^{-4}\,\mathrm{K^{-1}}$	ρ	$7200\,\mathrm{kg\,m^{-3}}$
γ	$1.2\,\mathrm{N\,m^{-1}}$	μ_0	$1.26\times10^{-6}\,\mathrm{H\,m^{-1}}$
μ	$0.006\,\mathrm{kg\,m^{-1}\,s^{-1}}$	σ	$7.7\times10^{5}\,\Omega^{-1}\,\mathrm{m^{-1}}$
$\mathrm{d}\gamma/\mathrm{d}T$	$10^{-4}\,\mathrm{N\,m^{-1}\,K^{-1}}$	ε	0.9
C_P	$753\,\mathrm{J\,kg^{-1}\,K^{-1}}$	ΔH	$2.47\times10^{5}\,\mathrm{J\,kg^{-1}}$
T_l	1723 K	T_s	1523 K
k	$20\,\mathrm{W\,m^{-1}\,K^{-1}}$	K_{max}	$10^{4}\,\mathrm{s^{-1}}$

The conservation of radial momentum is

$$\frac{\partial}{\partial t}(\rho u)+\frac{1}{r}\frac{\partial}{\partial r}\left(\rho ruu-\mu r\frac{\partial u}{\partial r}\right)+\frac{\partial}{\partial z}\left(\rho uw-\mu\frac{\partial u}{\partial z}\right)$$
$$=-\frac{\partial P}{\partial r}+\frac{1}{r}\frac{\partial}{\partial r}\left(\mu r\frac{\partial u}{\partial r}\right)-2\mu\frac{u}{r^2}+\frac{\partial}{\partial z}\left(\mu\frac{\partial w}{\partial r}\right)$$
$$-j_z B_\theta-Ku. \tag{2}$$

The conservation of axial momentum is

$$\frac{\partial}{\partial t}(\rho w)+\frac{1}{r}\frac{\partial}{\partial r}\left(\rho ruw-\mu r\frac{\partial w}{\partial r}\right)+\frac{\partial}{\partial z}\left(\rho ww-\mu\frac{\partial w}{\partial z}\right)$$
$$=-\frac{\partial P}{\partial z}+\frac{1}{r}\frac{\partial}{\partial r}\left(\mu r\frac{\partial u}{\partial z}\right)+\frac{\partial}{\partial z}\left(\mu\frac{\partial w}{\partial z}\right)$$
$$+j_r B_\theta-Kw+\rho g\beta(T-T_r). \tag{3}$$

The temperature-dependent drag term which represents fluid flow in the mushy zone is incorporated into the momentum equation via $-Ku$ and $-Kw$, where

$$K=\begin{cases}0 & T>T_l\\ K_{max}(T_l-T)/(T_l-T_s) & T_s\le T\le T_l\\ \infty & T<T_s.\end{cases} \tag{4}$$

The conservation of energy is

$$\frac{\partial}{\partial t}(\rho h)+\frac{1}{r}\frac{\partial}{\partial r}\left(\rho ruh-r\frac{k}{C_p}\frac{\partial h}{\partial r}\right)+\frac{\partial}{\partial z}\left(\rho wh-\frac{k}{C_p}\frac{\partial h}{\partial z}\right)$$
$$=-\Delta H\frac{\partial f_L}{\partial t}. \tag{5}$$

In the energy equation, the latent heat of fusion is included by employing the liquid fraction, f_L, which is defined as follows:

$$f_L=\begin{cases}1 & T>T_l\\ (T-T_s)/(T_l-T_s) & T_s\le T\le T_l\\ 0 & T<T_s\end{cases} \tag{6}$$

where T_l and T_s are the liquidus and solidus temperature, respectively.

The conservation of electrical charge is given as follows. In order to obtain the electromagnetic force terms in equations (2) and (3), the electrical potential ϕ is calculated by solving the equation for the current's continuity,

$$\frac{1}{r}\frac{\partial}{\partial r}\left(\sigma r\frac{\partial\phi}{\partial r}\right)+\frac{\partial}{\partial z}\left(\sigma\frac{\partial\phi}{\partial z}\right)=0 \tag{7}$$

and the current density is calculated from Ohm's law,

$$j_r=-\sigma\frac{\partial\phi}{\partial r}\qquad j_z=-\sigma\frac{\partial\phi}{\partial z} \tag{8}$$

while the self-induced azimuthal magnetic field B_θ is derived from Ampère's law:

$$B_\theta=\frac{\mu_0}{r}\int_0^r j_z r\,\mathrm{d}r. \tag{9}$$

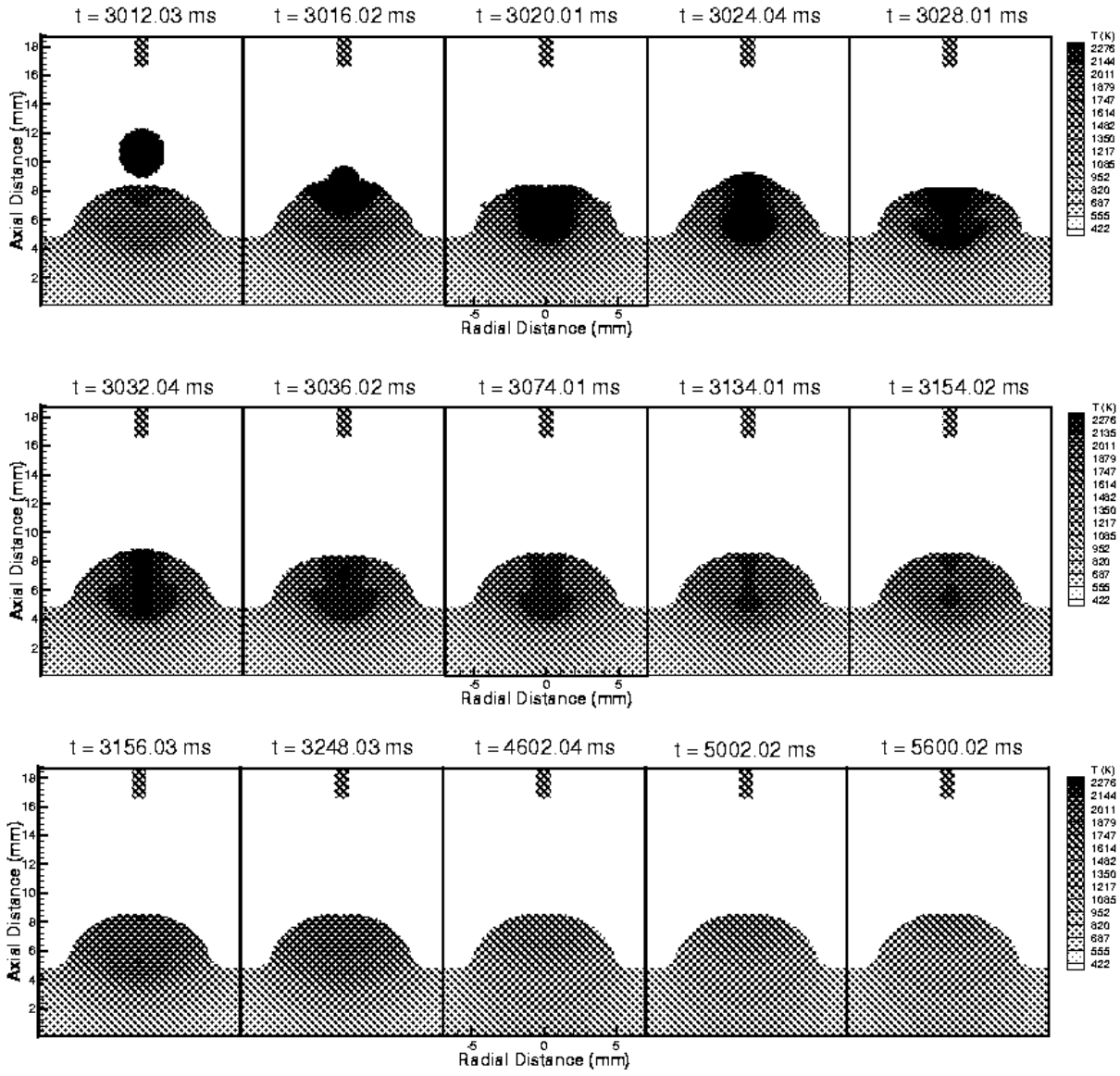

(a)

Figure 9. (a) The temperature distribution for the impingement of the last droplet and subsequent solidification (case B). (b) The velocity distribution for the impingement of the last droplet and subsequent solidification (case B).

3.2. Tracking of free surfaces

The moving free surface is tracked using a volume-of-fluid function, F, which represents the volume of fluid in the computational cell. The function F takes the value of 1 for the cell filled with the fluid and becomes 0 for the empty cell. If the cell is located on the free surface, the function F has a value between 0 and 1. The function F is governed by the equation

$$\frac{\partial F}{\partial t} + \frac{1}{r}\frac{\partial}{\partial r}(ruF) + \frac{\partial}{\partial z}(wF) = 0. \qquad (10)$$

In addition, there are some numerical techniques to handle the free surface such as the surface pressure due to curvature and the effect of wall adhesion. These are discussed in detail by Nichols *et al* [13] and will not be reiterated here.

3.3. Boundary conditions

3.3.1. Boundary conditions for momentum. The boundary conditions needed to specify the fluid-flow problem are

(i) the symmetry about the centreline,
(ii) that there is no slip at the solid boundaries and
(iii) that surface-tension-driven flow at the free surface, is described by

$$\tau_s = \mu\frac{\partial V_s}{\partial n} = \frac{\mathrm{d}\gamma}{\mathrm{d}T}\frac{\partial T}{\partial s}. \qquad (11)$$

3.3.2. Boundary conditions for thermal energy. The boundary conditions pertaining to the heat-transfer problem are

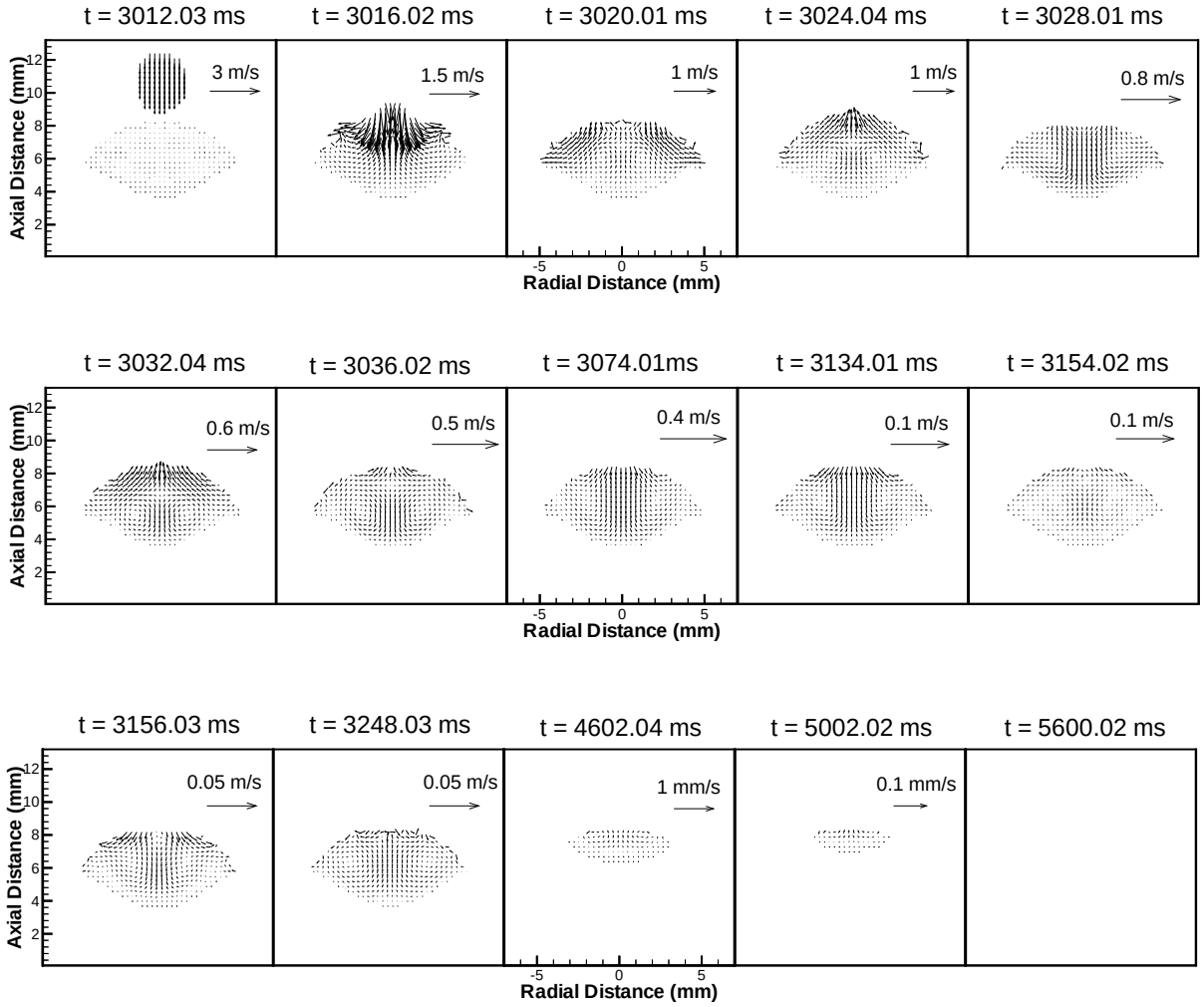

(b)

Figure 9. (Continued)

(i) the symmetry about the axial centreline

(ii) the heat flux from the welding arc at the free surface is assumed to obey a Gaussian-type distribution of the form

$$-k\frac{\partial T}{\partial n} = \frac{\eta U I}{2\pi r_q^2}\exp\left(-\frac{r^2}{2r_q^2}\right) - h_c(T - T_\infty) \qquad (12)$$

where h_c is a combined heat-transfer coefficient for the radiative and convective boundary expressed in the equation [18]

$$h_c = 24.1 \times 10^{-4}\varepsilon T^{1.61} \qquad (13)$$

and (iii) the boundary conditions for the surfaces without heat input are expressed as

$$-k\frac{\partial T}{\partial n} = h_c(T - T_\infty). \qquad (14)$$

3.3.3. Electrical potential boundary conditions. The boundary conditions concerning the electrical potential are

(i) the symmetry about the centreline,

(ii) an isopotential line ($\phi = 0$) is selected at the right wall because the right wall is far from the weld pool ($\partial\phi/\partial z = 0$ is set at the bottom wall) and

(iii) at the free surface, an assumed Gaussian-type current flux is described by

$$-\sigma\frac{\partial\phi}{\partial n} = \frac{I}{2\pi r_c^2}\exp\left(-\frac{r^2}{2r_c^2}\right). \qquad (15)$$

4. Results and discussion

4.1. Case A

4.1.1. Arc striking and the first droplet after arc ignition. The welding arc is struck by touching the workpiece with the end of the wire. As shown in figure 2, when the wire touches the weld metal, the end of the wire melts because of the Joule heating. Molten metal spreads gradually on the metal surface. At the beginning, the rate of the wire's melting is slower than the wire-feeding speed; thus, there is no space for arc ignition between the electrode and the workpiece. During the time of a short

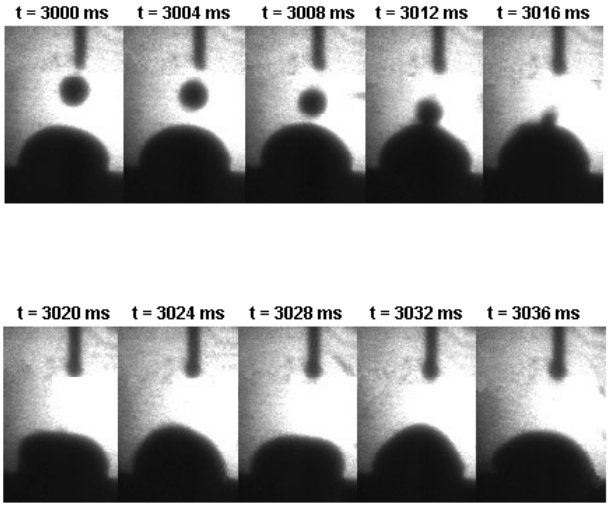

Figure 10. The image for the impingement of the last droplet onto the molten pool (case B).

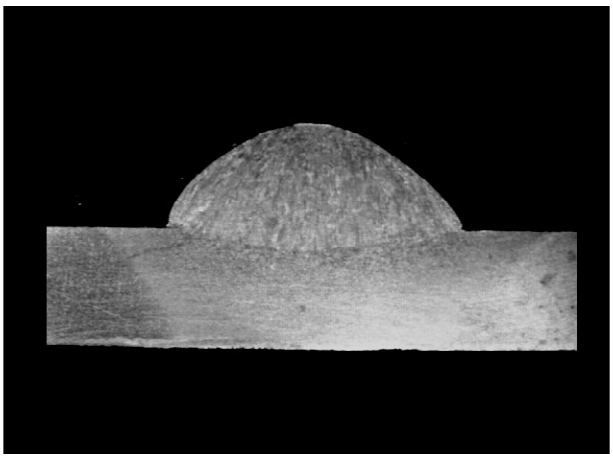

Figure 11. The cross section of the resultant weld bead (case B).

circuit, the electrode is overheated. It is shown that the hot wire collapses after around 92 ms. At the same time, the welding arc is struck. In the model, the wire is assumed to be at the liquidus temperature (T_l) and the velocity of the fluid is assumed to be equal to the wire-feeding speed. After the collapse, the fluid flow is controlled by the buoyancy, electromagnetic force and surface tension. That is to say, the governing equations used are the same as those mentioned before. Figure 3 indicates that the predicted surface profile of the weld pool in the process of arc striking under the above-mentioned assumptions agrees well with the experimental results.

After 240 ms, the first droplet is formed and detached from the wire. The droplet's velocity is increased after acceleration across the arc. As shown in figure 3, when the droplet transfers to the pool it imparts kinetic energy to a region local to the surface and this kinetic energy is expended in generating a cavity. Then the fluid is accelerated into that cavity by the hydrostatic, electromagnetic and surface-tension forces [19]; therefore, the cavity fills immediately after impact. Owing to the droplet recoiling and the inwards impingement of fluid at the centre, the fluid moves upwards, as shown in figure 3(b). A hump, affected by the inertial force, which overpasses the equilibrium point, is formed. That is, part of the kinetic energy has been transformed into potential energy. Under the impact of the above-mentioned forces, the fluid has to move downwards. Between the impingement of two successive drops, this loop will continue until equilibrium is achieved. This is called weld-pool oscillation.

4.1.2. The last droplet and subsequent solidification. After around 3 s, the arc is extinguished in order to observe the impact of the last droplet and subsequent solidification. Figure 4 shows that, when the droplet impinges upon the weld pool, there is a mixing of mass, momentum and energy between the droplet and the molten pool. The addition of the molten droplet increases the volume of the weld pool, the impact of the droplet causes a marked indentation in the weld pool and the heat contained in the overheated droplet is transferred to the weld pool. The added high-temperature filler metal is driven downwards by the stirring force due to the momentum of the droplets falling onto the pool. Some experiments [20] have led one to conclude that, with GMA welding, the arc heat influences the depth of penetration only to a limited degree. As shown in figure 4(a), the high-temperature filler metal could reach the bottom of the weld pool, which suggests that the penetration of the weld pool could be mainly determined by the impingement of droplets. Without additional droplets and arc heating, the molten pool becomes smaller and smaller and the solidification is completed after around 6 s. The size of the molten pool and the flow pattern are shown in figure 4(b). The flow pattern in the weld pool makes the effect of convection on heat transfer and weld-pool oscillation easily understood. It is also shown that the impingement of droplets is a key factor affecting the fluid velocity. The fluid's velocity increases significantly after impingement and decreases gradually during the process of solidification.

The experimental images are shown in figure 5. Although the cavity in the centre of the weld pool could not be observed under the current experimental conditions, the obtained images show that the weld-pool oscillation could be triggered by the impingement of a droplet and that the amplitude of oscillation is decreased gradually.

The resultant weld bead is shown in figure 6. The actual penetration is less than the predicted results in figure 4(b), and the penetration is not finger-like. In the model, we assume that the droplets always impact upon the centre of the molten pool. In actual stationary gas metal arc welding, the transfer of metal could not be focused on one point. The droplets strike the weld pool over a wide area. As a result, there is no finger-shaped penetration. Since the weld surface's profile is controlled by surface tension and the locations of impact of the drops on the workpiece are not a dominant factor, the predicted surface profile agrees well with the resultant weld bead.

4.2. Case B

4.2.1. Impingement of a droplet on a substrate. Figure 7 depicts the behaviour of a molten droplet impacting on the substrate. It is seen that the droplet assumed to be spherical is accelerated in the arc plasma. After the droplet hits the substrate surface, it spreads out on the substrate's surface quickly. As shown, the velocity of fluid flow in the molten pool rapidly decreases. An examination of the temperature contours in figure 7(a) reveals that the substrate in the central region is more molten than is that on the splat's periphery due to its higher fluid temperature. This is because the splat's periphery is continuously cooled by being in contact with the low-temperature surface of the substrate as it spreads outwards. The heat input from the welding arc is another factor affecting the temperature distribution. To get the image of a droplet impinging on the substrate, the workpiece is moved forwards quickly after the arc is struck. As shown in figure 8, the experimental results are in reasonable agreement with predictions. The instant when the workpiece stops is set as $t = 0$ ms in figure 8.

4.2.2. The last droplet and subsequent solidification. In GMAW, hot, molten droplets are continuously supplied to the centre of the weld pool. At the current of 160 A, the size of the droplet is much bigger and the velocity of the droplet is less. As shown in figure 9, the frequency of weld-pool oscillation is greater than that in case A. This may be due to the drop's velocity at the moment of impact being different. At higher current, the cavity caused by the impingement of the droplet is much deeper and it takes longer to fill. Comparing with figure 3, the solidification process is described in detail in figure 9. The heat loss is mainly from the base metal, so the liquid adjacent to the solid–liquid interface solidifies first. The last liquid zone is located in the top of the weld bead. The predications are in fair agreement with the corresponding experimental images shown in figure 10.

The cross section of a weld bead at 160 A is shown in figure 11. Compared with case A, the penetration is shallow. In gas metal arc spot welding, the periodically injected droplets result in a high-reinforcement bead profile. Since it is difficult for falling droplets to reach the bottom of the weld pool because of the bead's height, the heat cannot be transferred to the weld's root efficiently. This is the reason why GMAW could be used in rapid prototyping, which needs higher weld beads and shallower penetration. For welding, the increase in the droplet-transfer rate could cause the well-known finger-shaped penetration. With increasing droplet-transfer rate, the droplets are more easily directed to one point. The cavity caused by the impingement of the droplets could not be filled in time because of the higher droplet-transfer rate. The droplets fall constantly in the same cavity so that the heat is transferred efficiently to the weld's root.

5. Conclusions

The globular transfer in stationary gas metal arc welding has been dynamically simulated using a modified SOLA-VOF method. The principal conclusions are summarized as follows.

In the process of arc striking, the collapse of the overheated wire has been observed and simulated. The weld pool's oscillation could be triggered by the impingement of the droplets. The frequency and amplitude of the pool's oscillation is closely connected with the momentum of droplets.

The droplet-transfer frequency has a major influence on the weld pool's configuration. A higher frequency leads to a deeper penetration. The locations where the droplets impinge on the weld pool are another important factor that affects the pool's shape. The scatter of impinging locations could result in a shallower and wider weld shape instead of the normal finger shape.

The calculated temperature distribution reveals that the fluid's temperature around the periphery is lower than the temperature at the centre. Solidification, therefore, is expected to initiate from the solid–liquid interface and advance towards the centre. It is noticed that the velocity of falling droplets is an important factor in deciding the velocity field in the molten pool.

A high-speed video camera has been used to record the images of the metal-transfer process. The calculated results appear to agree well with the experimental results.

Acknowledgments

This work was supported by the National Science Foundation of the USA under grant numbers DMI-9732848 and THECB/ATP, grant No 003613-005 which is gratefully acknowledged. The authors also appreciate the assistance of Dr B Zheng, I Kmecko and M Labudovic in experiments.

References

[1] Lei Y P and Shi Y W 1994 Numerical treatment of the boundary conditions and sources terms on a spot welding process with combining buoyancy-maragoni-driven flow *Numerical Heat Transfer* B **26** 455–71

[2] Zacharia T, David S A, Vitek J M and DebRoy T 1989 Weld pool development during GTA and laser beam welding of type 304 stainless steel, part I – theoretical analysis *Welding J.* **68** 499–509s

[3] Zacharia T, Eraslan A H and Aidun D K 1988 Modeling of non-autogenous welding *Welding J.* **67** 18–27s

[4] Zacharia T, Eraslan A H and Aidun D K 1988 Modeling of autogenous welding *Welding J.* **67** 53–62s

[5] Tsai M C and Kou S 1990 Electromagnetic-force-induced convection in weld pools with a free surface *Welding J.* **69** 241–6s

[6] Kim S D and Na S J 1992 Effect of weld pool deformation on weld penetration in stationary gas tungsten arc welding *Welding J.* **71** 179–93s

[7] Zacharia T, David S A, Vitek J M and Kraus H G 1991 Computational modeling of stationary gas-tungsten-arc weld pools and comparison to stainless steel 304 experimental results *Metall. Trans.* B **22** 243–57

[8] Tsao K C and Wu C S 1988 Fluid flow and heat transfer in GMA weld pools *Welding J.* **67** 70–5s
[9] Kim J W and Na S J 1994 A study on the three-dimensional analysis of heat and fluid flow in GMAW using boundary-fitted coordinates *Trans. ASME* **116** 78–85
[10] Ushio M and Wu C S 1997 Mathematical modeling of three-dimensional heat and fluid flow in a moving gas metal arc weld pool *Metall. Trans.* B **28** 509–17
[11] Choi S K, Ko S H, Yoo C D and Kim Y S 1998 Dynamic simulation of metal transfer in GMAW – part 2: short-circuit transfer mode *Welding J.* **77** 45–51s
[12] Trapaga G, Matthys E F, Valencia J J and Szekely J 1992 Fluid flow, heat transfer, and solidification of molten metal droplets impinging on substrates: comparison of numerical and experimental results *Metall. Trans.* B **23** 701–18
[13] Nichols B D, Hirt C W and Hotchkiss R S 1980 SOLA-VOF: a solution algorithm for transient fluid flow with multiple free boundaries, report LA-8355, Los Alamos Scientific Laboratory
[14] Haidar J and Lowke J J 1996 Predictions of metal droplet formation in arc welding *J. Phys. D: Appl. Phys.* **29** 2951–60
[15] Lesnewich A 1958 Control of melting rate and metal transfer in gas shielded metal arc welding: Part 1 *Welding J.* **37** 343–53s
Lesnewich A 1958 Part 2 *Welding J.* **37** 418–25s
[16] Rnee S and Kannatey-ashibu E Jr 1992 Observation of metal transfer during gas metal arc welding *Welding J.* **72** 381–6s
[17] Lancaster J F 1986 *The Physics of Welding* (Oxford: Pergamon)
[18] Goldak J, Bibby M, Moore J and Patel B 1986 Computer modeling of heat flow in welds *Metall. Trans.* B **17** 587–600
[19] Nemchinsky V A 1996 The distribution of the electromagnetic force in a welding pool *J. Phys. D: Appl. Phys.* **29** 2659–63
[20] Essers W G and Walter R 1981 Heat transfer and penetration mechanisms with GMA and plasma-GMAW *Welding J.* **61** 37–58s